Modeling of the Complex between Transducin and Photoactivated Rhodopsin, a Prototypical G-Protein-Coupled Receptor†

Gregory V. Nikiforovich,* Christina M. Taylor, and Garland R. Marshall

Center for Computational Biology and Department of Biochemistry and Molecular Biophysics, Washington University Medical School, St. Louis, Missouri 63110

Received January 29, 2007; Revised Manuscript Received February 28, 2007

ABSTRACT: Obtaining a reliable 3D model for the complex formed by photoactivated rhodopsin (R*) and its G-protein, transducin (Gt$\alpha\beta\gamma$), would significantly benefit the entire field of structural biology of G-protein-coupled receptors (GPCRs). In this study, we have performed extensive configurational sampling for the isolated C-terminal fragment of the α-subunit of transducin, Gtα 340−350, within cavities of photoactivated rhodopsin formed by different energetically feasible conformations of the intracellular loops. Our results suggested a new 3D model of the rhodopsin−transducin complex that fully satisfied all available experimental data on site-directed mutagenesis of rhodopsin and Gt$\alpha\beta\gamma$ as well as data from disulfide-linking experiments. Importantly, the experimental data were not used as a priori constraints in model building. We performed a thorough comparison of existing computational models of the rhodopsin−transducin complex with each other and with current experimental data. It was found that different models suggest interactions with different molecules in the rhodopsin oligomer, that providing valuable guidance in design of specific novel experimental studies of the R*−Gt$\alpha\beta\gamma$ complex. Finally, we demonstrated that the isolated Gtα 340−350 fragment does not necessarily bind rhodopsin in the same binding mode as the same segment in intact Gtα.

G-protein-coupled receptors (GPCRs)[1] comprise the largest protein superfamily in humans (*1*). A typical GPCR consists of a single protein chain embedded in the cell membrane with seven helical transmembrane stretches (TM helices) connected by intracellular and extracellular loops (the IC and EC loops). In addition, GPCRs contain an extracellular N-terminal segment (often glycosylated) and an intracellular C-terminal segment. GPCRs trigger a variety of physiological functions by transducing an extracellular event, typically binding of an agonist ligand (neurotransmitter, peptide hormone, etc.), to an intracellular signal, such as cyclic AMP. Specifically, binding an agonist initiates conformational transitions from the resting state of the receptor to the activated state exposing the intracellular binding site for a heterotrimeric G-protein, a complex of α-, β-, and γ-subunits. Since GPCRs represent about 50% of targets for drugs currently in use (*2*), knowledge of the detailed 3D structures of activated GPCRs and their complexes with the corresponding G-proteins would be extremely relevant to wide areas of biochemistry, biophysics, and medicinal chemistry.

In this regard, special attention has recently been focused on rhodopsin, the 348-residue photoreceptor of the visual system. So far, extensive direct experimental spectroscopic data for both resting and activated states are available only for this GPCR. The 3D structures of dark-adapted rhodopsin (the R state) have been repeatedly determined by X-ray crystallography (*3*−*7*), and the structure of the transmembrane (TM) region of rhodopsin in the light-adapted state (the MII state, which corresponds to the activated R* state; see below) was deduced from data on site-directed spin labeling in solution (*8*). The 3D structure of the MI state of rhodopsin (the photoactivation state that precedes MII; see below) in a crystal was resolved by electron microscopy (*9*), and recently, the 3D structure of the MII state was suggested by X-ray crystallography (*10*). Since the largest GPCR family (family A, up to 700 members) displays distinct sequential homology to rhodopsin (*1, 11*), the X-ray structure of dark-adapted rhodopsin has been used as a template for building 3D structures of other rhodopsin-like GPCRs in their inactive states [see, e.g., a minireview (*12*)]. A 3D model of the activated R* state of rhodopsin in solution was also considered as a possible model for a conserved mechanism of activation of GPCRs (*13*).

Contrary to other GPCRs, however, rhodopsin is activated not by binding an extracellular ligand but by a single photon of light of the correct wavelength. Upon exposure to light, 11-*cis*-retinal, covalently attached to K296 in TM7, isomerizes to all-*trans*-retinal. Experimentally distinguishable stages of the photoactivation cycle are as follows (*14*): from the PHOTO state, where all-*trans*-retinal is highly distorted, to the BATHO state, then to the LUMI state (at this stage, all-

†This work was partly supported by NIH Grants GM 68460, GM53630, and EY1211301 (G.V.N. and G.R.M.) and by NIH Institutional National Research Service Award 5-T32-EY13360-06 from the National Eye Institute and a W. M. Keck Fellowship in Molecular Medicine (C.M.T.).

* To whom correspondence should be addressed. Telephone: (314) 362-1566. Fax: (314) 362-0234. E-mail: gregory@ccb.wustl.edu.

[1] Abbreviations: GPCR, G-protein-coupled receptor; R, inactive rhodopsin; R*, activated rhodopsin; Gt$\alpha\beta\gamma$, trimeric transducin; Gtα, α-subunit of transducin; Gtβ, β-subunit of transducin; Gtγ, γ-subunit of transducin; MII, meta II state of rhodopsin; TM, transmembrane helix; IC, intracellular loop; EC, extracellular loop; AMP, adenosine monophosphate; ATP, adenosine triphosphate; PDB, Protein Data Bank.

10.1021/bi700185p CCC: $37.00
Published on Web 03/31/2007

trans-retinal is presumably no longer distorted), then to the meta I (MI) state, and, finally, to the meta II (MII) state. In the MII state, the Schiff base of retinal is unprotonated; at this stage photoactivated rhodopsin (R*) binds its G-protein transducin and triggers the visual transduction process. Therefore, the MII state represents, on one hand, the distinct state in the photoactivation cycle characterized by a specific shift of the wavelength of chromophore absorption and, on the other hand, the photoactivated R* state of rhodopsin that can bind transducin. Obviously, this latter capacity is of most significance for studies of rhodopsin as a prototypical GPCR and, specifically, for studies of possible 3D models of the recognition of transducin by the intracellular binding site of R*.

High-resolution experimental data on the rhodopsin−transducin complex are not available. Though the X-ray structures for trimeric transducin (Gt$\alpha\beta\gamma$) (*15*) as well as that of the α-subunit (Gtα) (*16*) and $\beta\gamma$-subunits (Gt$\beta\gamma$−phosducin complex) (*17*) are known, the important C-terminal fragments of the α- and γ-subunits (Gtα 340−350 and Gtγ 60−71) were unresolved in these X-ray crystal structures. There is also some discrepancy between the MII structure of rhodopsin suggested by X-ray crystallography and considerable biophysical experimental data. While the model deduced from site-directed spin labeling suggests possible tilt and rotation of the TM6 helix along the long transmembrane axis in solution (*8*, *19*) [by ca. 120° according to computational study (*18*)] or similar rearrangement in the intracellular TM region, the X-ray structure of the MII state did not show significant changes in the orientation of TM helices (*10*). Also, different X-ray structures of dark-adapted rhodopsin (the R state) displayed distinctly different conformers of IC loops (*3*−*7*) mainly due to their high conformational flexibility. Therefore, 3D models of the rhodopsin−transducin interaction cannot be directly deduced from the available experimental data. At the same time, 3D structures suggested by molecular modeling can account for a variety of IC loop conformations that likely exist in the R* state of rhodopsin.

In this study, we explored different possible 3D models for a complex between transducin and the R* state of rhodopsin. These models resulted from extensive sampling of configurations of the experimentally determined structure of the Gtα 340−350 fragment (*20*) within the cavities formed by various sets of low-energy conformers of the IC loops of rhodopsin obtained previously (*21*). It should be specifically noted that the goal of our study was not to suggest a highly detailed atomic resolution 3D model of the R*−transducin complex but rather to develop an energetically feasible working model consistent with available experimental data that could be tested by further experiments. In this regard, the 3D models suggested by our study were validated by comparison with experimental data and with models proposed by others.

METHODS

General Docking Protocol. The procedure of docking the Gtα 340−350 fragment, Ile^{340}-Lys^{341}-Glu^{342}-Asn^{343}-Leu^{344}-Lys^{345}-Asp^{346}-Cys^{347}-Gly^{348}-Leu^{349}-Phe^{350}, to the intracellular region of the activated rhodopsin consisted, basically, of packing together five fragments, namely, the rhodopsin sequences 61−75 (IC1), 136−153 (IC2), 222−249 (IC3), and 303−322 (IC4, the TM7 helical stem and helix H8) and Gtα 340−350. The packing protocol was essentially the same as that used earlier for energy calculations of the TM region of rhodopsin (*18*) and for packing the IC1 + IC2 + IC3 + H8 intracellular "package" (*21*). In brief, starting configurations of Gtα 340−350 in the cavity formed by the intracellular loops IC1, IC2, IC3, and H8 were adjusted by energy minimization in the multidimensional space of "global" and "local" coordinates. Each fragment was allowed to move as a rigid body in six dimensions corresponding to global coordinates (three orthogonal translations *X*, *Y*, and *Z* and three orthogonal rotations Tx, Ty, and Tz around the axes connected to the central point of the fragment). The local coordinates were the dihedral angles of the side chains for all five fragments. Spatial positions of side chains were optimized and reoptimized at each convergence step of energy minimization by an algorithm developed previously (*22*). During energy minimization, the dihedral angle values for the peptide backbones of the fragments were kept fixed; this assumption corresponded to a model of "hard cores" (rigid backbone dihedral angles) and "soft shells" (flexible dihedral angles of side chains) for each fragment (*18*, *23*).

Starting Conformations of the IC Loops and Gtα 340−350. Starting conformations of the intracellular region of the activated state of rhodopsin [that differed from the dark-adapted state by rotation of TM6 along the long axis at ca. 120°, as was suggested earlier (*18*)] were obtained in a previous study (*21*). The 3D structure of the peptide backbone of Gtα 340−350 used for docking procedures was that deduced earlier from transfer NOE measurements (*20*).

Force Field and Details of Energy Calculation. Energy calculations employed the ECEPP/2 force field (*24*, *25*) with rigid valence geometry and planar *trans*-peptide groups (except those for prolines, where the ω angles varied). Arg, Lys, Glu, and Asp side chains were considered as charged species. Energy calculations were performed with two different values of the macroscopic dielectric constant, $\epsilon = 2$ and $\epsilon = 80$ (see below in the Results section). All IC loops included the four-residue helical stems of the corresponding TM helices and were capped by acetyl or *N*-methyl groups at their N- or C-terminals, respectively. The Gtα 340−350 fragment was also capped with the *N*-acetyl and C-terminal COOH groups, respectively, to mimic the same fragment in the entire Gα subunit, where the N-terminal residue I340 is connected to the rest of Gtα.

Typically, two types of energy calculations were performed for each configuration of Gtα340−350. The "simplified energy calculations" comprised energy minimization in the space of the global coordinates along with optimization and reoptimization of spatial arrangements for each side chain at each convergence step of energy minimization by an algorithm developed previously (*22*). "Full energy calculations" involved energy minimization not only in the space of the global coordinates but also over the dihedral angles of the side chains.

Sampling of Gtα 340−350 Configurations. Sampling of possible six-dimensional configurations of Gtα 340−350 within the intracellular cavity of rhodopsin employed the Gtα 340−350 position suggested in a study by Filipek et al. (*26*) as a reference point and was performed in four main steps. First, the initial configurations of Gtα 340−350 were selected

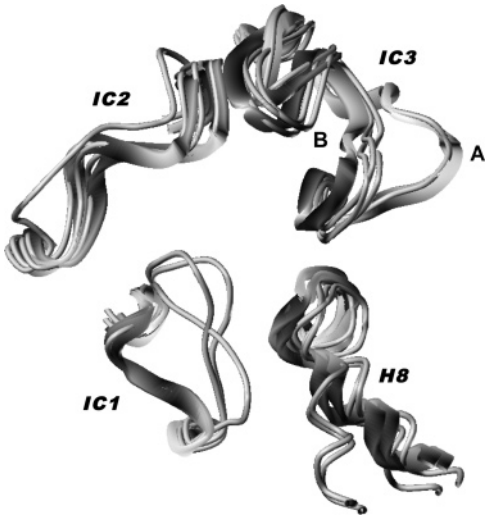

FIGURE 1: Sketch of the most open cluster of conformations of the IC loops deduced in Nikiforovich and Marshall (*21*). Traces of backbone conformations are shown as tubes. Conformations A and B used in this study are shown as shaded ribbons. The view is normal to the intracellular membrane surface.

by visual inspection on the grid of ΔX, ΔY, and ΔZ (relative to the reference point) with a step of 1 Å. For those configurations not sterically clashing with the IC loops of rhodopsin, orientations of Gtα 340−350 with ΔTx and ΔTy of −90°, −45°, 0°, 45°, and 90° and ΔTz (the helical axis of Gtα 340−350) of 12 values from 0° to 330° with an interval of 30° were considered. Each combination of all six coordinates was used then as a starting point for simplified energy calculations performed for the package of the five fragments (i.e., IC1, IC2, IC3, IC4, and Gtα 340−350). This step yielded low-energy configurations selected by an arbitrary energy cutoff (see Results). Second, new sets of initial configurations were created by sampling the vicinity of each selected configuration on the three-dimensional grid with the steps of ΔX, ΔY, and ΔZ equal to ±1 Å. For each of these initial configurations, full energy minimization with an energy convergence limit of 5 kcal/mol was performed. Third, full energy minimization with the same convergence limit was additionally performed for the 999 top-scoring initial configurations obtained by docking Gtα 340−350 to the intracellular loop package employing the program GRAMM for low-resolution docking (*27*) with the following parameters: grid step, 3.0; repulsion, 6.5; attraction, 0.0; potential range type, grid_step; projection, gray; representation, all; angle for rotations, 20. Fourth, resulting low-energy configurations from the previous two steps were pooled together, and a new round of full minimization with a finer energy convergence limit of 1 kcal/mol was performed.

RESULTS

*Gtα 340−350 within the Cavity Formed by the IC Loops of R**. It was logical to employ the 3D structures of the intracellular loops belonging to the "most open" cluster of conformations obtained previously by energy calculations [see the IC clusters differing by the rms cutoff of 3 Å described by Nikiforovich and Marshall (*21*)] as the starting points for docking procedure. Six conformations comprising this cluster are somewhat different in spatial orientations of the specific IC loops and H8 (see Figure 1). The two most different conformations that correspond to the most distant orientations of the largest IC3 loop were denoted as conformations A and B (see Figure 1). Interestingly, the X-ray snapshot of the structure of the IC3 loop in the photoactivated rhodopsin proposed by the recent study (*10*) was close to that in conformation B (data not shown). Both conformations A and B were selected for energy calculations to account for flexibility of the loops within the most open cluster. Accordingly, the docking procedures were run independently for conformations A and B. Also, since the energy calculations did not explicitly involve interactions of the IC loops or Gtα 340−350 with the charged membrane lipids and/or water, an accurate description of electrostatic interactions in the system was uncertain. To alleviate this problem, at least in part, one can consider duplicate energy calculations with two different values of the macroscopic dielectric constant, $\epsilon = 2$ and $\epsilon = 80$. The former value is standard in the ECEPP force field, and the latter simulates an aqueous environment by dampening electrostatic interactions between the charged functional groups. Therefore, to account for various uncertainties of the force field and the starting conformations of the IC loops, we decided to perform four independent runs of the entire docking procedure, namely, runs A2 (conformation A with $\epsilon = 2$), A80 (conformation A with $\epsilon = 80$), B2 (conformation B with $\epsilon = 2$), and B80 (conformation B with $\epsilon = 80$).

The independent runs of simplified energy calculations in configurational space for Gtα 340−350 corresponding to loop conformation A started with 5400 initial configurations and yielded 162 and 208 potentially low-energy configurations selected for further consideration (for A2 and A80, respectively). An arbitrary energy cutoff of $\Delta E = E - E_{min} \leq 70$ kcal/mol for the case with $\epsilon = 2$ and of $\Delta E \leq 30$ kcal/mol for the case with $\epsilon = 80$, respectively, was used. The difference between the two cutoffs reflected the fact that the range of energies of configurations calculated with $\epsilon = 2$ was much wider than that of configurations calculated with $\epsilon = 80$. Full energy calculations were then performed in the vicinity of each selected configuration, as well as for 999 configurations docked using the GRAMM procedure (see Methods). Totally, configurational sampling performed for Gtα 340−350 in the cavity corresponding to loop conformation A yielded 65 and 58 low-energy configurations (cases A2 and A80, respectively). Two independent runs were performed with loop conformation B exactly as those described for loop conformation A. These runs started with 12000 initial configurations and yielded 105 and 86 low-energy configurations of Gtα 340−350 for B2 and B80, respectively.

Generally, the relative spatial positions of fragments IC1, IC2, IC3, and IC4 (i.e., six global coordinates for each fragment) were only slightly changed as a result of energy minimization. At the same time, final configurations of Gtα 340−350 obtained for each of the independent runs displayed a wide variety of possible orientations of Gtα 340−350 within the intracellular cavity of photoactivated rhodopsin. Figure 2 depicts representatives of the clusters of the final configurations of Gtα 340−350 obtained by comparing relative positions of the heavy atoms of the peptide backbone with an rms cutoff of 3 Å in each case. One can see that configurations of Gtα 340−350 oriented somewhat normal to the membrane surface predominated for case A2, with

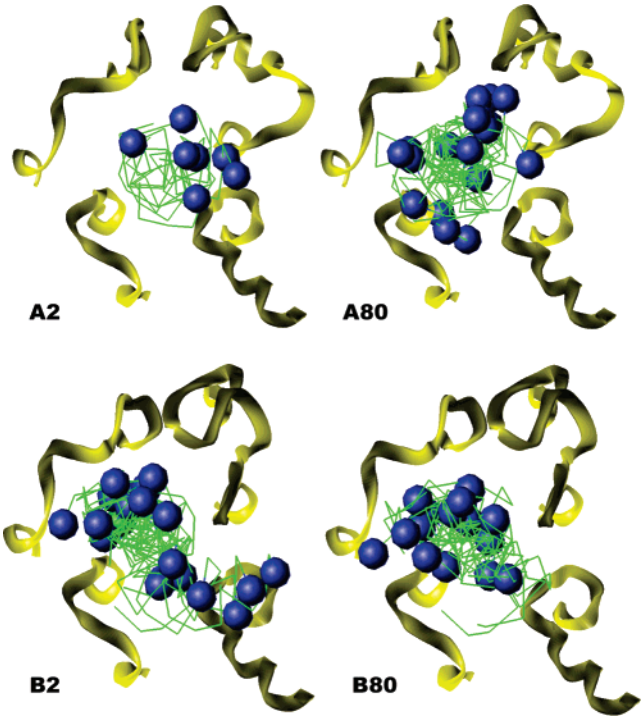

FIGURE 2: Representatives of different clusters of Gtα 340−350 configurations found for cases A2 (7 clusters), A80 (20 clusters), B2 (20 clusters), and B80 (16 clusters). Loops are shown as shaded ribbons. Gtα 340−350 molecules are shown as Cα traces in green; the N-terminal Cα atoms are shown as blue spheres. The view is normal to the intracellular membrane surface.

the N-terminal residue I340 being directed "outward" from the cavity between loops. In all other cases, A80, B2, and B80, the configurations were oriented in many different ways, including positions normal to the membrane surface with the N-terminal fragment directed both outward and inward from the cavity, as well as configurations oriented "across" the cavity, or more parallel to the membrane.

Tentative 3D Models of the R−Gtαβγ Complex.* Obviously, only low-energy configurations with the orientation of N-terminal residues of Gtα 340−350 facing outward from the binding cavity of R* could be employed for building a tentative 3D model of the complete R*−Gtαβγ complex. Totally, there were seven clusters of such configurations for case A2 **(**by the rms cutoff of 1 Å), 20 for A80, 20 for B2, and 16 for B80; see also Figure 2. For the lowest energy configuration of each cluster, the X-ray structure of Gtαβγ [the 1GOT entry in the PDB (*15*)] was overlapped with residues 340−343 of Gtα 340−350, and the C-terminal end of the γ-subunit (fragment Gtγ 60−71) was manually restored from the NMR-deduced structure (*28*) by overlapping with residues 60−62 in the X-ray structure of the γ-subunit. Then, helical stems of the IC loops were aligned to one of the rhodopsin molecules present in the tetrameric model of rhodopsin in the membrane [the PDB entry 1N3M (*29*, *30*); see also below], which allowed visualization of different orientations of the Gtαβγ molecule (corresponding to various configurations of Gtα 340−350) relative to the intracellular surface of the membrane. Many configurations were eliminated from further consideration, since visual inspection of these models displayed significant insertions of either Gtα or Gtβγ within the membrane and/or severe steric overlap with rhodopsin itself. However, nine configurations from case A2, six configurations from A80, one from B2, and 3 from B80 produced tentative 3D models of the R*−Gtαβγ without any obvious unrealistic features.

The above 3D models were predicted by molecular modeling without applying any experimental data on possible interactions between R* and Gtαβγ as constraints. These 3D structures represented different plausible models of the R*−Gtαβγ complex, the most plausible ones to be selected by compatibility with currently available experimental data, derived primarily from site-directed mutagenesis and disulfide-linking experiments. For instance, two independent alanine scans of the α-subunit of transducin implicated several residues of Gtα as being involved in direct contact with rhodopsin (*31*, *32*). Specifically, residues Gtα V214, R309, D311, V312, K313, F330, F332, D337, I338, I340, K341, N343, L344, G348, L349, and F350 were indicated in one study (*31*) and residues Gtα L344 and L349 in another (*32*). The alanine scan data agreed also with the data on competition in binding to R* between Gtαβγ and the fragments Gtα 311−328 and Gtα 340−350 (*33*). Possible contacts of the Gtα 309−313 fragment with R* were confirmed also by disulfide-linking experiments that suggested contacts between fragment Gtα 310−313 and the S240 residue (IC3) of photoactivated rhodopsin (*34*).

Experimental data on cross-linking, however, also suggested contacts between S240 of R* and the N-terminal fragment Gtα 19−28 (*35*), and the alanine scan data on Gtγ indicated that residues Gtγ 62−64 may contact R* as well (*36*). Simultaneous contacts of both the C-terminal fragment Gtα 310−313 and the N-terminal fragment Gtα 19−28 with the same S240 were not allowed by the X-ray structure of the heterotrimeric transducin (1GOT), since residues 19−28 were located in the long α-helical stretch that pointed away from the bulk of the α-subunit and tightly interacted with the β-subunit. The same considerations were true regarding fragment Gtγ 62−64, which was far away from Gtα 340−350 in 1GOT, being closer to Gtα 19−28.

At the same time, recent studies by electron and atomic force microscopy showed that in native membranes rhodopsin molecules may form dimers that, in turn, align in rows one dimer wide, with each row contacting another parallel one (*29*, *30*). The 3D model of packed rows of rhodopsin molecules is available in the PDB as entry 1N3M. We have used this model to explore which tentative arrangements of Gtαβγ predicted in this study would satisfy the above experimentally suggested contacts with R*, assuming that Gtα fragments 309−313, 330−338, and 340−350 contacted one molecule of rhodopsin and fragments Gtα 19−28 and Gtγ 62−64 contacted an adjacent molecule.

Certainly, all computational models involved some contacts between R* and Gtα 340−350. Table 1 contains the values for four characteristic Cα−Cα distances calculated for the tentative R*−Gtαβγ models between residues Gtα K131−R* S240, Gtα D337−R* S144, Gtα L19−R* S240, and Gtγ P63−R* C316. The last two distances were calculated for the rhodopsin molecule adjacent to that interacting with Gtα 340−350; the two molecules belong to different parallel rows in 1N3M. With reasonable assumption that only Cα−Cα distances smaller than 20 Å can provide for contacts between residues of R* and Gtαβγ, Table 1 clearly shows that only three models that originated from case A2 adequately agreed with all experimental data

Table 1: Characteristic Cα−Cα Distances in the Tentative 3D Models of the R*−Gtα$\beta\gamma$ Complex

model	Gtα K313− R* S240	Gtα D337− R* S144	Gtα L19− R* S240[a]	Gtγ P63− R* C316[a]
A2	13.1	9.6	14.0	***20.9***
	13.2	11.0	15.5	***22.5***
	12.4	9.7	15.6	***22.1***
*	10.4	8.6	10.5	14.9
*	8.7	9.1	10.7	15.2
	16.7	9.2	***22.9***	***33.1***
	15.1	8.8	17.1	***23.5***
**[b]	13.3	8.8	11.9	16.0
	14.1	11.8	16.6	***22.7***
A80	14.2	11.4	18.1	***26.3***
	13.1	11.2	18.7	***26.8***
	22.7	9.9	***33.1***	***58.1***
	22.0	11.0	***33.8***	***58.6***
	15.1	6.9	***31.7***	***55.8***
	13.6	12.2	19.8	***60.0***
B2	16.5	13.3	10.3	***42.6***
B80	***32.1***	19.5	***37.7***	***81.3***
	12.0	12.9	19.8	***57.9***
	14.6	13.5	18.6	***58.5***

[a] Residue in the adjacent molecule of rhodopsin. [b] The double asterisk marks the selected representative model.

discussed above (marked by asterisks in Table 1; distances larger than 20 Å are shown in bold in Table 1).

Representative 3D Model of the R−Gtα$\beta\gamma$ Complex.* Configurations of Gtα 340−350 in the three A2 models that satisfy the experimental data were very similar to each other, differing only in slight shifts (by 0.9−1.5 Å) among the translational coordinates *X*, *Y*, *Z* of Gtα 340−350. As a representative, we selected the model featuring direct contacts between residues of Gtα 340−350 and fragments 136−139, 247−251, and 310−312 in R* (marked by a double asterisk in Table 1). These contacts were suggested by data on rhodopsin mutants stabilized in the MII state either by isolated Gtα 340−350 [mutations in fragments 136−139 and 247−251 (*37*)] or by both isolated Gtα 340−350 and Gtα$\beta\gamma$ [mutations in fragment 310−312 (*38*, *39*)]. Our representative model contained close contacts between some side chain atoms of Gtα F350/rhodopsin V138, Gtα K345/rhodopsin E249, and Gtα K345/rhodopsin K311. The pairs of residues of Gtα 340−350 and rhodopsin were considered to be in close contact when at least one distance between any atoms of the residue side chains was less than 4.5 Å.

Our representative model also agrees well with additional experimental data. Rather recently, modifications of rhodopsin residues 226, 229, and 230 in IC3 (*40*, *41*), 242−244 in IC3 (*41*), and even 313 and 317 in H8 (*41*) were suggested to influence the interaction of rhodopsin with the C-terminal fragment Gtα 340−350 but not necessarily by direct contacts to residues of Gtα 340−350. The representative model displayed the contact Gtα E342/rhodopsin Q244, as well as the less pronounced contacts Gtα F350/rhodopsin V230 and Gtα K341/E342/rhodopsin Q244 (for these two contacts, the calculated atom−atom distances were less than 6.5 Å).

Figure 3 shows the discussed close contacts between R* residues and residues of Gtα 340−350 corresponding to the chosen representative 3D model of Gtα$\beta\gamma$−R*. As previously mentioned, the experimental data on the alanine scan of Gtα suggest that residues most involved in interaction with R* are I340, K341, N343, L344, G348, L349, and F350.

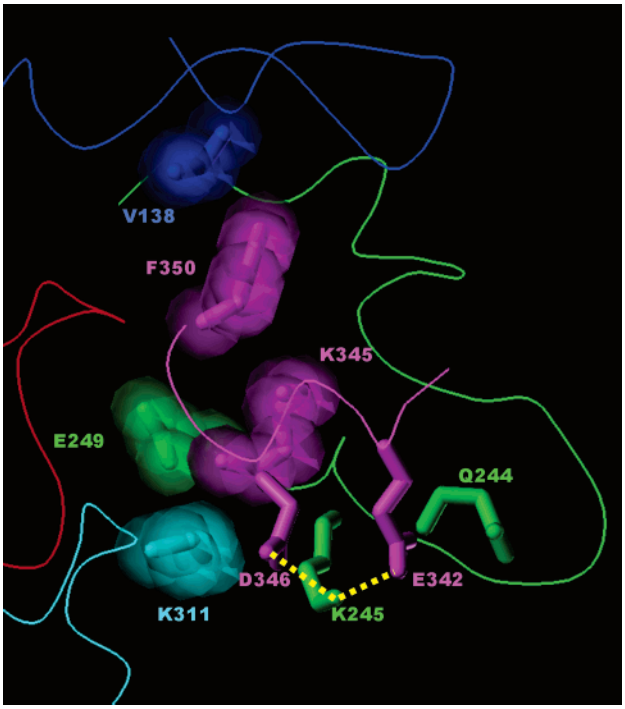

FIGURE 3: Sketch of contacts between residues of Gtα 340−350 and rhodopsin in the representative 3D model of the R*−Gtα complex. The view is along the membrane plane. The backbones of IC loops are shown as one-line ribbons in red (IC1), blue (IC2), green (IC3), and cyan (IC4), and the backbone of Gtα 340−350 is shown in magenta. Only side chains mentioned in the text are shown as capped sticks. They are colored and labeled according to the colors of IC loops and Gtα 340−350. Side chains involved in contacts Gtα F350/R* V138, Gtα K345/R* E249, and Gtα K345/R* K311 are additionally shown as transparent space-filled models. The hydrogen bonds between the side chains of D346/E342 and K245 are shown as yellow dashed lines.

In the representative model, almost all of the Gtα 340−350 residues are involved in contacts with R* residues, with the notable exception of Gtα C347 (data not shown). The system of contacts in Figure 3 also rationalizes why single mutations of Gtα E342, K345, and D346 for alanine did not show an impaired wild-type phenotype for Gtα$\beta\gamma$ in site-directed mutagenesis studies (*31*). The β-carboxyl group of D346 and the γ-carboxyl group of E342 are simultaneously involved in a strong hydrogen-bonding interaction with the ϵ-amino group of rhodopsin residue K245 (see Figure 3); therefore, elimination of only one of them may weaken, but not interrupt, the strong interactions with K245. On the other hand, elimination of the side chain of Gtα K345 would break hydrogen bonding with the side chain of E249 in R*, but it would be not enough to disturb the configuration of Gtα stabilized with the strong interaction between Gtα E342/D346 and K245 in R*.

Figure 4 presents the entire representative 3D model Gtα$\beta\gamma$−R* complex consistent with all current experimental data on interactions between Gtα$\beta\gamma$ and R*. Though unrefined, this complex constitutes a reliable working model of photoactivated rhodopsin bound to transducin.

DISCUSSION

Comparison with Models of the Gtα$\beta\gamma$−R Complex Developed by Others.* To our knowledge, three other groups have previously developed 3D models for the complex of

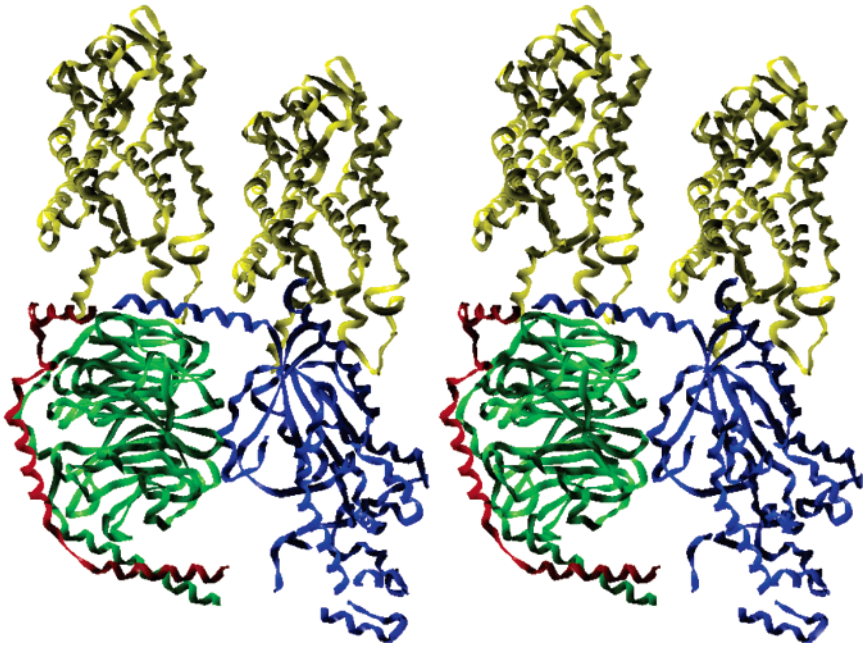

FIGURE 4: Stereoview of the deduced model of the rhodopsin(s)−transducin complex. The Gtα subunit is shown as a shadowed ribbon in blue, Gtβ in green, and Gtγ in red. Rhodopsins are shown in yellow.

rhodopsin with Gt$\alpha\beta\gamma$ at atomic resolution by molecular modeling (*26*, *42*−*45*). These models were obtained by docking of the X-ray structure of Gt$\alpha\beta\gamma$ (1GOT), where the unordered segments (Gtα 340−350 and Gtγ 60−71) were restored according to the structures deduced from transfer NOE measurements (*20*, *28*) to generate rhodopsin models employing various protocols.

The study by Fanelli and Dell'Orco assumed that Gt$\alpha\beta\gamma$ initially recognizes rhodopsin in the dark-adapted R state, and the two molecules form a so-called "precoupled" complex R−Gt$\alpha\beta\gamma$ (*42*). Accordingly, the dark-adapted X-ray structure of rhodopsin [the PDB entry 1U19 (*6*)] was selected as a starting model for rhodopsin; in this X-ray structure, the specific conformations of all IC loops were resolved. Several options of Gt$\alpha\beta\gamma$ differing by some mutations were docked to rhodopsin by the rigid-body docking algorithm ZDOCK, and the highest scoring solutions that satisfied the Cα−Cα distance constraints (between residues S240 in rhodopsin and Gtα N343/D311, rhodopsin R135 and Gtα F350, and rhodopsin Q312 and Gtα K345) were subjected to energy minimization employing the CHARMM force field. The resulting structure of the complex [the Gt_*mut1* model (*42*)] is depicted in Figure 5, panel B.

The study led by Filipek and Palczewski started from the rhodopsin tetramer structure deduced from the experimental data of atomic force microscopy (the PDB entry 1N3M, the same used in our study) (*26*). The authors modeled the missing loops of rhodopsin (PDB entry 1F88) with the commercially available INSIGHT package; the TM region of the rhodopsin molecule in the R* state (the molecule interacting with Gtα 340−350) was modeled by rotation of TM6 by 120° along the long axis. Gt$\alpha\beta\gamma$ was manually fit to the rhodopsin tetramer, and MD simulations of the entire system (up to 100 ps) that included explicit membrane phospholipids molecules followed. Figure 5 (panel C) depicts this model. As in our model, Gt$\alpha\beta\gamma$ interacts with two rhodopsin molecules; however, in this case the rhodopsin molecule interacting with Gtα 340−350 and the adjacent

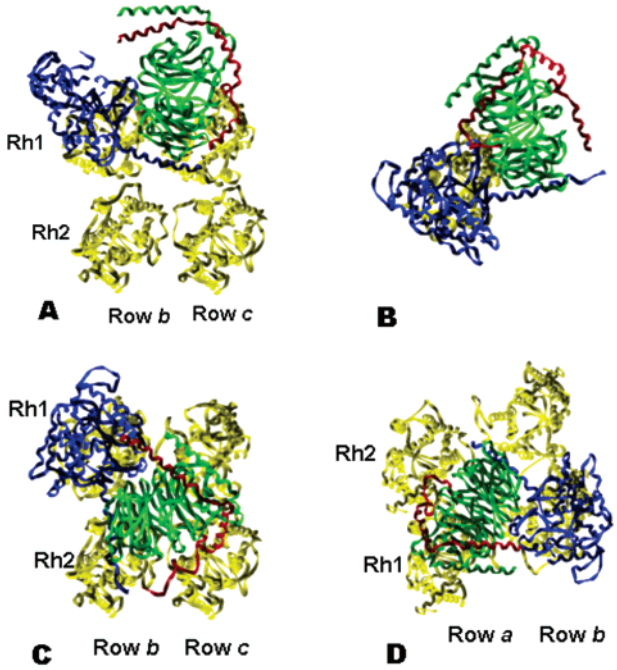

FIGURE 5: Comparison of the 3D models developed in our study (A), in ref *42* (B), in ref *26* (C), and in ref *45* (D). The view is normal to the intracellular surface of the membrane. Colors are the same as in Figure 4. Rhodopsin molecules are labeled to show molecules belonging to the same dimer (Rh1 or Rh2) and to the same row (row a, row b, or row c). Note the different packing of rhodopsin molecules in panel D. TM regions of Rh1, row b, for all models are overlapped.

one that interacts with Gtγ 60−71 both belong to the rhodopsin dimer in the same row (Rh1, row b; Rh 2, row b). Recent refinement of this model (longer MD simulation of up to 500 ps) resulted in a few relatively insignificant changes (*43*).

In the study led by Ciarkowski, one molecule of rhodopsin was complexed to one molecule of Gt$\alpha\beta\gamma$ (*44*). The TM region of rhodopsin in the R* state was modeled by applying experimental constraints obtained by site-directed spin label-

Table 2: Characteristic Cα−Cα Distances in the 3D Models of the R*−Gtα$\beta\gamma$ Complex

model	Gtα K313− R* S240	Gtα D337− R* S144	Gtα L19− R* S240[a]	Gtγ P63− R* C316[a]
Figure 5, panel A	13.3	8.8	11.9	16.0
Figure 5, panel B	9.1	12.4	n/a	n/a
Figure 5, panel C	***21.5***	17.0	***20.0***	16.0
Figure 5, panel D	***24.1***	***29.1***	16.8	17.5

[a] Residue in the adjacent molecule of rhodopsin.

ing (*8*) to the 3D structure of the R state; the missing loops were modeled with the commercially available SYBYL package. Gtα$\beta\gamma$ was manually aligned to the resulting model of R*, and the total system (one molecule of rhodopsin and one molecule of transducin) was subjected to unconstrained molecular dynamics (10 ns) in a fully hydrated lipid bilayer. Further development of the model followed, where the six oligomers of rhodopsin were repacked in the manner still consistent with findings from atomic force microscopy but different from that of 1N3M (*45*). In this model, Gtα$\beta\gamma$ also contacts two molecules of rhodopsin but not the same molecules as suggested either by our model or by the model developed by Filipek et al. (*26*) (see panel D in Figure 5). Very recently, extensive MD simulations (up to 5.3 ns) were performed to refine this model (Witt et al., submitted for publication); however, no significant changes were observed.

Table 2 lists the values of the four characteristic Cα−Cα distances calculated for the models depicted in Figure 5. The same distances were used above to estimate whether the tentative models of the R*−Gtα$\beta\gamma$ complex deduced in our study satisfy the experimental data that suggested contacts of R* with fragments Gtα 19−28, 309−313, and 330−338 and Gtγ 62−64. One can see that only in one model by the other authors (Figure 5, panel B) all calculated distances were smaller than the cutoff assumed for possible contact (distance less than 20 Å). On the other hand, the side chains of residues Gtα I340, K341, and N343, which were suggested to contact rhodopsin based on the data of the alanine scan of Gtα (*31*), do not display such contacts in the model in Figure 5, panel B. Note, however, that the experimental data (*31*) reflected the final stage of activation of Gtα$\beta\gamma$ by R*, whereas the focus of the study by Fanelli and Dell'Orco was the "precoupling" stage (*42*).

For the model by Filipek et al. (*26*) shown in Figure 5, panel C, two distances in Table 2 only slightly exceeded the cutoff of 20 Å. This model reproduced contacts of Gtα 340−350 with rhodopsin fragments 247−251 and 310−312 but not with 136−139. Also, residues Gtα K341, E342, K345, D346, L349, and F350 contacted some rhodopsin residues; interestingly, the side chains of E342 and D346 both were involved in a hydrogen-bonding interaction with an ϵ-amino group of lysine, as in our model (Figure 3), but in this case it was with K67. However, residues Gtα I340, N343, and L344 implicated in the interaction with rhodopsin by experimental data (*31*) were not in contact with any rhodopsin residue.

The model by Ciarkowski et al. (*45*) shown in Figure 5, panel D, is characterized by two distances over the cutoff of 20 Å (see Table 2). At the same time, this model featured experimentally suggested contacts of Gtα 340−350 with rhodopsin fragments 136−139, 247−251, and 310−312. It also correctly predicted involvement of all Gtα 340−350 residues in contact with rhodopsin, with the exception of D346, C347, and E342. However, recent experimental data suggested cross-linking between positions 175 and 206 in two different rhodopsin molecules that form a dimer (*46*); this feature is not compatible with rearrangement of rhodopsin oligomers suggested by panel D in Figure 5 but fits well to the 1N3M arrangement employed in our model and in the model developed by Filipek et al. (*26*) (panels A and C in Figure 5).

Generally, the three models depicted in Figure 5 differ from our model and from each other mainly by rotations of Gtα$\beta\gamma$ around the axis normal to the membrane surface placed in the cavity formed by the IC loops. As a result, the different models suggest interactions with different members of the rhodopsin tetramer. For the model in panel B, Gtα$\beta\gamma$ is rotated by ca. −45° relative to our model (panel A), which would require interactions with rhodopsins Rh1 (row b) and Rh2 (row c), had the second rhodopsin been present in model B. For panel C, the model is rotated by ca. 45° relative to our model, and Gtα$\beta\gamma$ is interacting with rhodopsins Rh1 (row b) and Rh2 (row b). For the model in panel D, this rotation is almost 180°, leading to interactions with Rh1 (row b) and Rh2 (row a). These differences between the models are significantly large to be reliably distinguished by direct structural experiments, i.e., cross-linking of rhodopsin mutants with mutants of Gtα$\beta\gamma$ or estimating intracomplex distances by inserting spin labels in both Gtα$\beta\gamma$ and rhodopsin (see also ref *47*). Emerging high-resolution NMR studies of the R*−Gtα$\beta\gamma$ complex also would be important in this regard (e.g., ref *48*).

Isolated Gtα 340−350 and the C-Terminal Fragment 340−350 of Gtα May Bind Rhodopsin in Different Binding Modes. A tacitly accepted hypothesis underlying the study of the C-terminus of Gtα is that the isolated undecapeptide Gtα 340−350 binds the activated state of rhodopsin in the same binding mode as when included in the entire Gtα as its C-terminal fragment. The hypothesis is supported mainly by the fact that the isolated Gtα 340−350 competes with Gtα$\beta\gamma$ for binding to light-activated rhodopsin and stabilizes the MII state in the photoactivation cycle (*33*, *49*, *50*). On the other hand, involvement of the C-terminal fragment of Gtα in direct interaction with rhodopsin and in stabilization of the MII state was indicated by site-directed mutagenesis (*31*, *32*) as well as by recent NMR study using semisynthetic Gtα subunits (*51*). Transfer NOE measurements have also shown that the isolated Gtα 340−350 acquires its definitive 3D structure only when complexed with light-activated rhodopsin (*20*, *33*, *52*, *53*); this structure, according to the same hypothesis, corresponds to the R*-bound structure of the C-terminal fragment of intact Gtα.

Our results, however, do not necessarily support this hypothesis. As depicted in Figure 2, many low-energy configurations of the isolated Gtα 340−350 fragment correspond to orientations "inward" or across the rhodopsin intracellular cavity, which are inconsistent with possible orientation of Gtα 340−350 as the C-terminal fragment of intact Gtα in complex with R*. These configurations were most often observed in cases A80 and B80, i.e., with ϵ = 80. This observation seems quite reasonable considering that the isolated fragment Gtα 340−350 in the rhodopsin cavity should be much more exposed to the intracellular aqueous environment than the same fragment in the tightly packed

Table 3: Direct Contacts between the Side Chains of Rhodopsin Fragments 136−139, 247−251, and 310−312 and Residues of Isolated Gtα 340−350 in Representative Configurations from Cases A2, A80, B2, and B80

	residues of Gtα 340−350									
	I340	K341	E342	N343	L344	K345	D346	C347	L349	F350
A2							K311			V138 E249 Q312
						E249	K311			V138
A80	E249 Q312	V137 V138								
		V138 E249 Q312								
				Q312				E249 Q312	V138 Q312	
B2				E249 Q312				V138	V137	
	V137 V138		Q310 Q312		V137 V138	Q312	E249 K311 Q312	E249		
	V137 V138		E249 N310 K311 Q312			Q312				
									V137 V138	E249 Q312
		E249 N310 Q312	V138 E249	V137		E249 K311 Q312				
						E249 N310 Q312	Q312			V137 V138 Q312
	V137		Q312	E249 Q312			Q312			
		V138 E249	V137 E249			E249 Q312				Q312
			V137				Q312	E249		
	E249 Q312	V138 E249 Q312								
B80		Q312			E249	E249 Q312				V138 E249
	E249 Q312	V137 V138 E249								
		V137 Q312				E249 Q312				
		V137	E249			E249 Q312	K311			
				Q312	Q312	V137		E249 Q312	E249 N310 Q312	V137 V138
									V137 V138	E249 Q312
		E249 Q312	V138 E249 Q312			E249 Q312				Q312
	V137 V138	E249 Q312								

intact R*−Gtα$\beta\gamma$ complex. Interestingly, alternative binding modes for Gtα 340−350 in complex with photoactivated rhodopsin agreed with available experimental data. For instance, it was well established by site-directed mutagenesis that residues of the isolated Gtα 340−350 peptide may be involved into direct contacts with fragments 136−139, 247−251 (*37*), and 310−312 (*38*) of rhodopsin. Such contacts (defined as above, with at least one atom−atom distance being less than 4.5 Å) were found in 9 configurations of Gtα 340−350 corresponding to case A2, 6 for A80, 11 for B2, and 29 for B80. These configurations were clustered by comparing relative positions of the heavy atoms of the peptide backbone with an rms cutoff of 3 Å yielding 2 different clusters for A2, 3 for A80, 10 for B2, and 8 for B80. Table 3 lists all direct contacts between rhodopsin fragments 136−139, 247−251, and 310−312 and residues of Gtα 340−350 for the lowest energy representatives of each cluster. It is obvious that, depending on which residues of Gtα 340−350 contact rhodopsin fragments 136−139, 247−251, and 310−312, multiple binding modes of Gtα 340−350 to R* can satisfy the above experimental data.

Thus, these results indicated that the assumption of identical binding modes for isolated Gtα 340−350 and the same fragment in the Gtα$\beta\gamma$−R* complex was not necessarily correct. One additional indication was the comparison of the experimental results on the alanine scan on the C-terminal fragment of Gtα (*31*) and the experimental data on structure−function relationships for isolated Gtα 340−350 (*49*, *50*). While the data on Gtα suggested that the residues most involved in interaction with R* were I340, K341, N343, L344, G348, L349, and F350, the data obtained by testing the combinatorial libraries for the isolated Gtα 340−350 (*49*), as well as other analogues of Gtα 340−350 (*50*, *54*), point to residues C347 and G348. Indeed, interactions of rhodopsin residues with Gtα C347, which are not present in our model, are rather frequent in Table 3 that relates to configurations of isolated Gtα 340−350. Interestingly, the binding configuration common for Gtα 340−350 and several analogues, suggested on the basis of a different protocol of molecular docking, also involved interaction of Gtα C347 with Q244 of rhodopsin (*65*). Recent data on site-directed mutagenesis showed also that replacement of K341 by leucine greatly enhances binding of isolated Gtα 340−350 to R* but virtually does not affect binding of the entire Gtα (*55*). Furthermore, significant stabilization of the MII state of rhodopsin was observed when the N-terminus of the isolated Gtα 340−350 was cross-linked to the C140 residue of rhodopsin (*56*), corresponding to a configuration totally forbidden for the C-terminal fragment of Gtα in complex with R*. Also, very recently, TrNOE studies of several synthetic analogues of Gtα 340−350 concluded that analogues may bind R* in different binding modes (*57*).

Besides Gtα 340−350, the farnesylated Gtγ 60−71 fragment (Gtγ 60−71-far) was also known to stabilize the MII state of rhodopsin and to compete with Gtα$\beta\gamma$ for binding to R* (*58*, *59*). As was already mentioned, these two peptide fragments are located too far from each other in the 3D structure of Gtα$\beta\gamma$ to interact with the same rhodopsin molecule. Therefore, an important feature of the R*−Gtα$\beta\gamma$ model deduced in this study was the interaction of Gtα$\beta\gamma$ with two molecules of rhodopsin instead of one, allowing interaction of Gtα 340−350 and Gtγ 60−71-far with two different rhodopsin molecules. However, since activation of rhodopsin is achieved by a single photon (*60*), which cannot activate two molecules of rhodopsin simultaneously, several mechanisms of Gtα$\beta\gamma$−rhodopsin interactions including that of sequential fit of Gtα 340−350 and Gtγ 60−71-far with two different sites on the same rhodopsin molecule were proposed [as was briefly reviewed (*36*)]. In our view, the most reliable way to substantiate any specific mechanism would require further experimental results; at the same time, by analogy with the situation for Gtα 340−350, one may assume that similar caveats to those discussed above should be considered in interpretation of the data on stabilization of the MII state by the isolated Gtγ 60−71-far. These caveats are supported with experimental finding that the isolated Gtγ 60−71-far, while effectively binding R*,

cannot replace the Gt$\beta\gamma$ complex in activating nucleotide exchange by Gt$\alpha\beta\gamma$ (*61*). Also, experimental studies interpreted the structural role of the farnesyl moiety in Gtγ rather differently, suggesting either involvement in specific interaction with R* (*28*) or anchoring other Gt subunits and/or the membrane (*62*, *63*). Finally, while one set of experiments suggested partial overlap of the binding sites on rhodopsin for Gtα 340−350 and Gtγ 60−71-far (*64*), other data provided evidence that these sites are distinctly different (*51*). Keeping all of the above in mind, proposed mechanisms of Gt$\alpha\beta\gamma$−rhodopsin interactions based on experiments on stabilization of the MII state employing isolated Gtα 340−350 and Gtγ 60−71-far could be significantly different from those based on direct experiments on intact Gt$\alpha\beta\gamma$ activation.

Concluding Remarks. Our modeling study was based on extensive configurational sampling performed for Gtα 340−350 within intracellular cavities of activated rhodopsin formed by different low-energy conformations of intracellular loops. The study deduced a working 3D model of the Gt$\alpha\beta\gamma$−rhodopsin complex that is consistent with all available experimental data obtained by site-directed mutagenesis of rhodopsin and Gt$\alpha\beta\gamma$, as well as by disulfide-linking experiments. Notably, these experimental results were used only as filters to select the most plausible models from those suggested by independent modeling and were not employed as constraints in building models. The proposed model agreed with experimental results despite several less rigorous assumptions made in the modeling protocol. On the other hand, the experimental results were not of high resolution themselves. The model proposed in this study fits experimental data better than other existing models; however, any final discrimination between our model and other models will require input of new experimental data, both from spectroscopy and site-directed mutagenesis.

Along with suggesting a model for the Gt$\alpha\beta\gamma$−rhodopsin complex, our study demonstrated that the isolated fragment Gtα 340−350 and the same fragment in the C-terminal part of Gtα can possess very different binding modes in the cavity formed by the IC loops of rhodopsin. This conclusion agrees with experimental observations that photostabilization of the MII state of rhodopsin can be achieved by the isolated Gtα 340−350 fragment in configurations incompatible with those of the C-terminal part of intact Gtα when complexed with rhodopsin. Together, these findings indicate that structural interpretations of experiments on peptide stabilization of the MII state and direct experiments on activating intact Gt$\alpha\beta\gamma$ may yield contradictory results. Since most of the available experimental data relate to stabilization of the MII state of rhodopsin by the isolated peptide Gtα 340−350, structural interpretation in terms of possible models of the Gt$\alpha\beta\gamma$−R* complex is, therefore, limited. Similar caveats may also apply in interpretation of experimental results on MII stabilization obtained with another important peptide fragment of transducin, Gtγ 60−71-far.

In summary, our study yielded several new results that contribute to understanding of structural aspects of GPCR biochemistry. First, we suggested the new 3D model of the rhodopsin−transducin complex that fully satisfies currently available experimental data. Second, we performed thorough comparisons of the existing computational models of the rhodopsin−transducin complex with each other and with experimental data. It was found that different models suggest interactions with different molecules in the rhodopsin oligomer, which may provide valuable guidance in the specific design of novel experimental studies of the R*−Gt$\alpha\beta\gamma$ complex. Third, we demonstrated that the isolated Gtα 340−350 fragment does not necessarily bind rhodopsin in the same binding mode as the same segment in Gtα.

ACKNOWLEDGMENT

The authors are indebted to Drs. Francesca Fanelli, Slawomir Filipek, and Jerzy Ciarkowski, who kindly provided us with the atomic coordinates of the models developed in refs *42*, *26*, and *44* and *45*, respectively, which made possible their comparison with the model suggested in this study. We are thankful also to Profs. Oleg G. Kisselev and Thomas J. Baranski for reading the manuscript and for valuable comments.

REFERENCES

1. Gether, U. (2000) Uncovering molecular mechanisms involved in activation of G protein-coupled receptors, *Endocr. Rev. 21*, 90−113.
2. Drews, J. (2000) Drug discovery: A historical perspective, *Science 287*, 1960−1964.
3. Palczewski, K., Kumasaka, T., Hori, T., Behnke, C. A., Motoshima, H., Fox, B. A., Le Trong, I., Teller, D. C., Okada, T., Stenkamp, R. E., Yamamoto, M., and Miyano, M. (2000) Crystal structure of rhodopsin: A G protein-coupled receptor, *Science 289*, 739−745.
4. Teller, D. C., Okada, T., Behnke, C. A., Palczewski, K., and Stenkamp, R. E. (2001) Advances in determination of a high-resoultion three-dimensional structure of rhodpsin, a model of G-protein-coupled receptors (GPCRs), *Biochemistry 40*, 7761−7772.
5. Okada, T., Fujiyoshi, Y., Silow, M., Navarro, J., Landau, E. M., and Shichida, Y. (2002) Functional role of internal water molecules in rhodopsin revealed by X-ray crystallography, *Proc. Natl. Acad. Sci. U.S.A. 99*, 5982−5987.
6. Okada, T., Sugihara, M., Bondar, A. N., Elstner, M., Entel, P., and Buss, V. (2004) The retinal conformation and its environment in rhodopsin in light of a new 2.2 Å crystal structure, *J. Mol. Biol. 342*, 571−583.
7. Li, J., Edwards, P. C., Burghammer, M., Villa, C., and Schertler, G. F. (2004) Structure of bovine rhodopsin in a trigonal crystal form, *J. Mol. Biol. 343*, 1409−1438.
8. Hubbell, W. L., Altenbach, C., and Khorana, H. G. (2003) Rhodopsin structure, dynamics and activation, *Adv. Protein Chem. 63*, 243−290.
9. Ruprecht, J. J., Mielke, T., Vogel, R., Villa, C., and Schertler, G. F. (2004) Electron crystallography reveals the structure of metarhodopsin I, *EMBO J. 23*, 3609−3620.
10. Salom, D., Lodowski, D. T., Stenkamp, R. E., Le Trong, I., Golczak, M., Jastrzebska, B., Harris, T., Ballesteros, J. A., and Palczewski, K. (2006) Crystal structure of a photoactivated deprotonated intermediate of rhodopsin, *Proc. Natl. Acad. Sci. U.S.A. 103*, 16123−16128.
11. Fredriksson, R., Lagerstrom, M. C., Lundin, L. G., and Schioth, H. B. (2003) The G-protein-coupled receptors in the human genome form five main families. Phylogenetic analysis, paralogon groups, and fingerprints, *Mol. Pharmacol. 63*, 1256−1272.
12. Ballesteros, J. A., Shi, L., and Javitch, J. A. (2001) Structural mimicry in G protein-coupled receptors: Implications of the high-resolution structure of rhodopsin for structure-function analysis of rhodopsin-like receptors, *Mol. Pharmacol. 60*, 1−19.
13. Khorana, H. G. (2000) Molecular biology of light transduction by the mammalian photoreceptor, rhodopsin, *J. Biomol. Struct. Dyn., Conversation 11*, 1−16.
14. Borhan, B., Souto, M. L., Imai, H., Shichida, Y., and Nakanishi, K. (2000) Movement of retinal along the visual transduction path, *Science 288*, 2209−2212.
15. Lambright, D. G., Sondek, J., Bohm, A., Skiba, N. P., Hamm, H. E., and Sigler, P. B. (1996) The 2.0 Å crystal structure of a heterotrimeric G protein, *Nature 379*, 311−319.

16. Lambright, D. G., Noel, J. P., Hamm, H. E., and Sigler, P. B. (1994) Structural determinants for activation of the alpha-subunit of α heterotrimeric G protein, *Nature 369*, 621−628.
17. Loew, A., Ho, Y. K., Blundell, T., and Bax, B. (1998) Phosducin induces a structural change in transducin beta gamma, *Structure 6*, 1007−1019.
18. Nikiforovich, G. V., and Marshall, G. R. (2003) 3D model for meta-II rhodopsin, an activated G-protein-coupled receptor, *Biochemistry 42*, 9110−9120.
19. Farrens, D. L., Altenbach, C., Yang, K., Hubbell, W. L., and Khorana, H. G. (1996) Requirement of rigid-body motion of transmembrane helices for light activation of rhodopsin, *Science 274*, 768−770.
20. Kisselev, O. G., Kao, J., Ponder, J. W., Fann, Y. C., Gautam, N., and Marshall, G. R. (1998) Light-activated rhodopsin induces structural binding motif in G protein alpha subunit, *Proc. Natl. Acad. Sci. U.S.A. 95*, 4270−4275.
21. Nikiforovich, G. V., and Marshall, G. R. (2005) Modeling flexible loops in the dark-adapted and activated states of rhodopsin, a prototypical G-protein-coupled receptor, *Biophys. J. 89*, 3780−3789.
22. Nikiforovich, G. V., Hruby, V. J., Prakash, O., and Gehrig, C. A. (1991) Topographical requirements for delta-selective opioid peptides, *Biopolymers 31*, 941−955.
23. Nikiforovich, G. V., Galaktionov, S., Balodis, J., and Marshall, G. R. (2001) Novel approach to computer modeling of seven-helical transmembrane proteins: Current progress in the test case of bacteriorhodopsin, *Acta Biochim. Pol. 48*, 53−64.
24. Dunfield, L. G., Burgess, A. W., and Scheraga, H. A. (1978) Energy parameters in polypeptides. 8. Empirical potential energy algorithm for the conformational analysis of large molecules, *J. Phys. Chem. 82*, 2609−2616.
25. Nemethy, G., Pottle, M. S., and Scheraga, H. A. (1983) Energy parameters in polypeptides. 9. Updating of geometrical parameters, nonbonded interactions, and hydrogen bond interactions for the naturally occuring amino acids, *J. Phys. Chem. 87*, 1883−1887.
26. Filipek, S., Krzysko, K. A., Fotiadis, D., Liang, Y., Saperstein, D. A., Engel, A., and Palczewski, K. (2004) A concept for G-protein activation by G protein-coupled receptor dimers: The transducin/rhodopsin interface, *Photochem. Photobiol. Sci. 3*, 628−638.
27. Vakser, I. A. (1996) Low-resolution docking: Prediction of complexes for underdetermined structures, *Biopolymers 39*, 455−464.
28. Kisselev, O. G., and Downs, M. A. (2003) Rhodopsin controls a conformational switch on the transducin gamma subunit, *Structure 11*, 367−373.
29. Liang, Y., Fotiadis, D., Filipek, S., Saperstein, D. A., Palczewski, K., and Engel, A. (2003) Organization of the G protein-coupled receptors rhodopsin and opsin in native membranes, *J. Biol. Chem. 278*, 21655−21662.
30. Fotiadis, D., Liang, Y., Filipek, S., Saperstein, D. A., Engel, A., and Palczewski, K. (2004) The G protein-coupled receptor rhodopsin in the native membrane, *FEBS Lett. 564*, 281−288.
31. Onrust, R., Herzmark, P., Chi, P., Garcia, P. D., Lichtarge, O., Kingsley, C., and Bourne, H. R. (1997) Receptor and betagamma binding sites in the alpha subunit of the retinal G protein transducin, *Science 275*, 381−384.
32. Osawa, S., and Weiss, E. R. (1995) The effect of carboxyl-terminal mutagenesis of Gt alpha on rhodopsin and guanine nucleotide binding, *J. Biol. Chem. 270*, 31052−31058.
33. Hamm, H. E., Deretic, D., Arendt, A., Hargrave, P. A., Koenig, B., and Hofmann, K. P. (1988) Site of G protein binding to rhodopsin mapped with synthetic peptides from the alpha subunit, *Science 241*, 832−835.
34. Cai, K., Itoh, Y., and Khorana, F. C. (2001) Mapping of contact sites in complex formation between transducin and light-activated rhodopsin by covalent crosslinking: Use of a photoactivatable reagent, *Proc. Natl. Acad. Sci. U.S.A. 98*, 4877−4882.
35. Itoh, Y., Cai, K., and Khorana, H. G. (2001) Mapping of contact sites in complex formation between light-activated rhodopsin and transducin by covalent crosslinking: Use of a chemically preactivated reagent, *Proc. Natl. Acad. Sci. U.S.A. 98*, 4883−4887.
36. Kisselev, O. G., and Downs, M. A. (2006) Rhodopsin-interacting surface of the transducin gamma subunit, *Biochemistry 45*, 9386−9392.
37. Acharya, S., Saad, Y., and Karnik, S. S. (1997) Transducin-α C-terminal peptide binding site consists of C-D and E-F loops of rhodopsin, *J. Biol. Chem. 272*, 6519−6524.
38. Marin, E. P., Krishna, A. G., Zvyaga, T. A., Isele, J., Siebert, F., and Sakmar, T. P. (2000) The amino terminus of the fourth cytoplasmic loop of rhodopsin modulates rhodopsin-transducin interaction, *J. Biol. Chem. 275*, 1930−1936.
39. Ernst, O. P., Meyer, C. K., Marin, E. P., Henklein, P., Fu, W. Y., Sakmar, T. P., and Hofmann, K. P. (2000) Mutation of the fourth cytoplasmic loop of rhodopsin affects binding of transducin and peptides derived from the carboxyl-terminal sequences of transducin alpha and gamma subunits, *J. Biol. Chem. 275*, 1937−1943.
40. Janz, J. M., and Farrens, D. L. (2004) Rhodopsin activation exposes a key hydrophobic binding site for the transducin alpha-subunit C terminus, *J. Biol. Chem. 279*, 29767−29773.
41. Natochin, M., Gasimov, K. G., Moussaif, M., and Artemyev, N. O. (2003) Rhodopsin determinants for transducin activation: A gain-of-function approach, *J. Biol. Chem. 278*, 37574−37581.
42. Fanelli, F., and Dell'Orco, D. (2005) Rhodopsin activation follows precoupling with transducin: Inferences from computational analysis, *Biochemistry 44*, 14695−14700.
43. Filipek, S. (2005) Organization of rhodopsin molecules in native membranes of rod cells—an old theoretical model compared to new experimental data, *J. Mol. Model. 11*, 385−391.
44. Slusarz, R., and Ciarkowski, J. (2004) Interaction of class A G protein-coupled receptors with G proteins, *Acta Biochim. Pol. 51*, 129−136.
45. Ciarkowski, J., Witt, M., and Slusarz, R. (2005) A hypothesis for GPCR activation, *J. Mol. Model. 11*, 407−415.
46. Kota, P., Reeves, P. J., Rajbhandary, U. L., and Khorana, H. G. (2006) Opsin is present as dimers in cos1 cells: Identification of amino acids at the dimeric interface, *Proc. Natl. Acad. Sci. U.S.A. 103*, 3054−3059.
47. Anderson, L. L., Marshall, G. R., Crocker, E., Smith, S. O., and Baranski, T. J. (2005) Motion of carboxyl terminus of Galpha is restricted upon G protein activation. A solution NMR study using semisynthetic Galpha subunits, *J. Biol. Chem. 280*, 31019−31026.
48. Ridge, K. D., Marino, J. P., Ngo, T., Ramon, E., Brabazon, D. M., and Abdulaev, N. G. (2006) NMR analysis of rhodopsin-transducin interactions, *Vision Res. 46*, 4482−4492.
49. Martin, E. L., Rens-Domiano, S., Schatz, P. J., and Hamm, H. E. (1996) Potent peptide analogues of a G protein receptor-binding region obtained with a combinatorial library, *J. Biol. Chem. 271*, 361−366.
50. Aris, L., Gilchrist, A., Rens-Domiano, S., Meyer, C., Schatz, P. J., Dratz, E. A., and Hamm, H. E. (2001) Structural requirements for the stabilization of metarhodopsin II by the C terminus of the alpha subunit of transducin, *J. Biol. Chem. 276*, 2333−2339.
51. Downs, M. A., Arimoto, R., Marshall, G. R., and Kisselev, O. G. (2006) G-protein alpha and beta-gamma subunits interact with conformationally distinct signaling states of rhodopsin, *Vision Res. 46*, 4442−4448.
52. Koenig, B. W., Mitchell, D. C., Konig, S., Grzesiek, S., Litman, B. J., and Bax, A. (2000) Measurement of dipolar couplings in a transducin peptide fragment weakly bound to oriented photo-activated rhodopsin, *J. Biomol. NMR 16*, 121−125.
53. Koenig, B., Kontaxis, G., Mitchell, D., Louis, J., Litman, B., and Bax, A. (2002) Structure and orientation of a G protein fragment in the receptor bound state from residual dipolar couplings, *J. Mol. Biol. 322*, 441.
54. Anderson, M. A., Ogbay, B., Arimoto, R., Sha, W., Kisselev, O. G., Cistola, D. P., and Marshall, G. R. (2006) Relative strength of cation-pi vs salt-bridge interactions: The Gtalpha(340−350) peptide/rhodopsin system, *J. Am. Chem. Soc. 128*, 7531−7541.
55. Herrmann, R., Heck, M., Henklein, P., Kleuss, C., Wray, V., Hofmann, K. P., and Ernst, O. P. (2006) Rhodopsin-transducin coupling: Role of the Ga C-terminus in nucleotide exchange catalysis, *Vision Res. 46*, 4582−4593.
56. Angel, T. E., Kraft, P. C., and Dratz, E. A. (2006) Metarhodopsin-II stabilization by crosslinked Gtalpha C-terminal peptides and implications for the mechanism of GPCR-G protein coupling, *Vision Res. 46*, 4547−4555.
57. Anderson, M. A., Ogbay, B., Kisselev, O. G., Cistola, D. P., and Marshall, G. R. (2006) Alternate binding mode of C-terminal phenethylamine analogs of G(t)alpha(340−350) to photoactivated rhodopsin, *Chem. Biol. Drug Des. 68*, 295−307.
58. Kisselev, O. G., Ermolaeva, M. V., and Gautam, N. (1994) A farnesylated domain in the G protein gamma subunit is a specific determinant of receptor coupling, *J. Biol. Chem. 269*, 21399−21402.

59. Kisselev, O., Pronin, A., Ermolaeva, M., and Gautam, N. (1995) Receptor-G protein coupling is established by a potential conformational switch in the beta gamma complex, *Proc. Natl. Acad. Sci. U.S.A. 92*, 9102−9106.
60. Baylor, D. A., Lamb, T. D., and Yau, K. W. (1979) Responses of retinal rods to single photons, *J. Physiol. 288*, 613−634.
61. Kisselev, O. G., Meyer, C. K., Heck, M., Ernst, O. P., and Hofmann, K. P. (1999) Signal transfer from rhodopsin to the G-protein: Evidence for a two-site sequential fit mechanism, *Proc. Natl. Acad. Sci. U.S.A. 96*, 4898−4903.
62. Hagiwara, K., Wada, A., Katadae, M., Ito, M., Ohya, Y., Casey, P. J., and Fukada, Y. (2004) Analysis of the molecular interaction of the farnesyl moiety of transducin through the use of a photoreactive farnesyl analogue, *Biochemistry 43*, 300−309.
63. Herrmann, R., Heck, M., Henklein, P., Hofmann, K. P., and Ernst, O. P. (2006) Signal transfer from GPCRs to G proteins: Role of the G alpha N-terminal region in rhodopsin-transducin coupling, *J. Biol. Chem. 281*, 30234−30241.
64. Herrmann, R., Heck, M., Henklein, P., Kleuss, C., Hofmann, K. P., and Ernst, O. P. (2004) Sequence of interactions in receptor-G protein coupling, *J. Biol. Chem. 279*, 24283−24290.
65. Taylor et al. (2007) *Biophys. J.* (in press).

BI700185P